Bound attractant at the leading vs. the trailing edge determines chemotactic prowess

Paul Herzmark*†, Kyle Campbell‡, Fei Wang*§, Kit Wong*, Hana El-Samad¶, Alex Groisman‡‖, and Henry R. Bourne*,**

Departments of *Cellular and Molecular Pharmacology and ¶Biochemistry and Biophysics, University of California, 600 16th Street, San Francisco, CA 94158; and ‡Department of Physics, University of California at San Diego, 9500 Gilman Drive, La Jolla, CA 92093

Contributed by Henry R. Bourne, July 2, 2007 (sent for review May 11, 2007)

We have analyzed chemotaxis of neutrophil-differentiated HL60 cells in microfluidic devices that create exponential gradients of the chemoattractant, f-Met-Leu-Phe (fMLP). Such gradients expose each cell to a difference in fMLP concentration (ΔC) across its diameter that is directly proportional to the ambient concentration (C) at that cell's position in the gradient, so the ratio $\Delta C/C$ is constant everywhere. Cells exposed to ambient fMLP concentrations near the constant of dissociation (K_d) for fMLP binding to its receptor (≈10 nM) crawl much less frequently when $\Delta C/C$ is 0.05 than when it is 0.09 or 0.13. Hence, cells can detect the gradient across their diameter without moving and, thus, without experiencing temporal changes in attractant concentration. At all $\Delta C/C$ ratios tested, the average chemotactic prowess of individual cells (indicated by the distance a cell traveled in the correct direction divided by the length of its migration path) is maximal for cells that start migrating at concentrations near the K_d and progressively decreases at higher or lower starting concentrations.

chemoattractant | gradient | neutrophils

An essential property of eukaryotic cells is their ability to orient in response to spatial cues. Only by correctly interpreting spatial changes in external stimuli can yeast cells mate, soil amoebae form spores, progeny of a fertilized egg form an organism, or neutrophils crawl toward their prey. Cells are known to respond to gradients of external stimuli such as chemoattractants, but how they sense and interpret gradients remains mysterious. The mystery goes beyond our ignorance of the biochemical basis of gradient sensing. More fundamentally, we have not even definitively identified the external cues sensed and interpreted by the cells and the respective roles of these cues in determining their responses to gradients.

Bacteria migrate up gradients of chemoattractants, in a process called chemotaxis. Chemotaxing bacteria assess gradients temporally, by moving through the attractant concentration field, sensing the local ambient concentration, comparing the concentration at a given moment with concentrations at previous times, and changing swimming behavior accordingly (1). It has been proposed that the larger cells of eukaryotes, in contrast, sense gradients at a given moment by comparing attractant concentrations at different positions on their surfaces and thus orient themselves to crawl in the up-gradient direction by interpreting the spatial cues present in their location at that moment. In other words, such cells assess the gradient spatially and respond to purely spatial cues by directed chemotactic migration. It has been shown that both neutrophils (2) and *Dictyostelium discoideum* amoebae (3) can sense relatively steep gradients of chemoattractant, supplied by a micropipette, without moving and therefore without comparing ambient concentrations in different locations. In both cases, immobile cells, paralyzed by treatments that block actin polymerization, accumulate phosphatidylinositol-3′,4′,5′-*tris*-phosphate (PIP3) at the up-gradient edge. In the micropipette experiments, however, the side of a cell that is first exposed to the attractant is also the side that will eventually be exposed to a higher attractant concentration. Thus, the spatial pattern of PIP3 accumulation might be influenced by this temporal pattern of application of attractant. Moreover, it remains unclear whether actual migration of these cells up a gradient can occur in response to purely spatial cues or requires that they move to different positions and compare the local concentrations of the attractant. This is particularly true when the gradients are relatively shallow as in traditional chemotaxis chambers. For example, Zigmond or Dunn chambers establish gradients quite slowly, over a period of ≈20 min (4, 5), which is longer than the time required for cells to polarize and orient their initial polarity (1–3 min) and long enough to allow them to migrate far from their starting positions to compare attractant concentrations at multiple locations.

In addition, we do not know how responses to gradients depend on the two most obvious potential external cues: the magnitude of the gradient at a given point vs. the ambient attractant concentration at that point. This problem was recognized by Zigmond (5, 6) >30 years ago, who studied gradient responses of neutrophils in a chemotactic chamber and quantified them by the degree of cell orientation in the up-gradient direction. She showed that orientation was most efficient for cells at ambient attractant concentrations near the apparent dissociation constant (K_d) of the cells' receptor for the attractant. Importantly, however, the ambient attractant concentration in those studies was only defined up to a 3× or 10× range, and the shape of the gradient varied between experiments and was not well controlled (5). Moreover, cell orientation was measured 30 min after the gradient was first applied, a period during which the shape of the gradient underwent substantial changes. Therefore, the results are hard to interpret or reproduce. In addition, as with all experiments in traditional chemotaxis devices, they do not discriminate between spatial and temporal modes of gradient interpretation.

To address both problems, one needs to generate concentration profiles with well defined shapes and to apply them quickly to cells. Generation of stable concentration profiles with linear or polynomial shapes has been enabled by recently developed microfluidic gradient-making networks (7–10), and by the use of

Author contributions: P.H. and H.R.B. designed research; P.H., F.W., and K.W. performed research; K.C. contributed new reagents/analytic tools; P.H., H.E.-S., A.G., and H.R.B. analyzed data; and P.H., H.E.-S., A.G., and H.R.B. wrote the paper.

The authors declare no conflict of interest.

Freely available online through the PNAS open access option.

Abbreviations: C, concentration; ΔC, difference in fMLP concentration; CI, chemotactic index; fMLP, f-Met-Leu-Phe.

†Present address: Department of Molecular and Cell Biology, University of California, 479 Life Science Addition, Berkeley, CA 94720-3200.

§Present address: University of Illinois, Chemical and Life Sciences Laboratory (CLSL), B107, 601 South Goodwin Avenue, Urbana, IL 61801.

‖To whom correspondence may be addressed at: University of California at San Diego, Urey Hall, MC 0374, 9500 Gilman Drive, La Jolla, CA 92093. E-mail: agroisman@ucsd.edu.

**To whom correspondence may be addressed at: University of California, N212F, Box 2140, 600 16th Street, San Francisco, CA 94158-2140. E-mail: bourne@cmp.ucsf.edu.

This article contains supporting information online at www.pnas.org/cgi/content/full/0705889104/DC1.

integrated microvalves (11), which allow such gradients to be imposed within a few seconds (12). Nevertheless, reports on chemotaxis in microfluidic devices have not addressed the issue of temporal vs. spatial sensing, whereas dependence of the efficiency of chemotaxis on attractant concentration, although discussed (9, 13, 14), has not been carefully studied.

The presence of a gradient leads to a difference in attractant concentrations, ΔC, across every cell in the gradient (for convenience we calculate ΔC in terms of a "standard" cell, assumed to be 10 μm in diameter). Most previous studies of chemotaxis in microfluidic devices required cells to interpret linear concentration profiles, where ΔC is constant at every point, whereas the ambient attractant concentration (C) increases linearly as a cell migrates up the gradient. As a result, the ratio of ΔC to C, that is, the fractional difference in concentration across the cell, hereafter referred to as D_c (= ΔC/C), decreases. Because recent experiments on yeast cells (15), neurons (16), and *D. discoideum* (3) suggest that these cells sense fractional rather than absolute differences in concentration, we felt it would be instructive to study chemotaxis in gradients in which D_c remains constant, regardless of C. This condition is met in exponential concentration profiles, in which the magnitude of the gradient is directly proportional to concentration at every point, so that D_c is constant.

Here, we present experiments on chemotactic responses of differentiated HL60 (dHL60) cells, a neutrophil-like cell line, to gradients of a tripeptide attractant, f-Met-Leu-Phe (fMLP). Like blood neutrophils, dHL60 cells can polarize not only in fMLP gradients but also in response to fMLP applied at a uniform concentration, lacking any spatial cue (17). We studied chemotactic responses of dHL60 cells in microfluidic devices that created either linear or exponential concentration profiles. The results show that dHL60 cells can detect and respond to purely spatial cues, and that their chemotactic prowess depends critically on both the gradient and the ambient attractant concentration. In a linear concentration profile, where ΔC is constant, chemotactic prowess steadily decreases with increasing concentration of attractant at the cell's starting position in the gradient, C_s, and prowess is maximal at the lowest C_s tested. In contrast, in exponential concentration profiles, where ΔC increases in proportion to C (D_c is constant), chemotactic prowess increases with C_s at low C_s, decreases with C_s at higher C_s, and is maximal at C_s values close to those reported for the dissociation constant of the fMLP-binding receptor ($K_d \approx 10$ nM). We tested exponential gradients with different D_c. For cells that start at a given C_s in these experiments, chemotaxis is more efficient when D_c is larger, that is, when the spatial cue, ΔC, is larger at any given C_s. Our results suggest that dHL60 cells translate the gradient and ambient concentration into chemotactic responses with the use of saturable attractant receptors to assess the difference between the numbers of receptors occupied by attractant at the cell's leading vs. its trailing edges.

Results

Chemotaxis in a Linear Gradient. We began by investigating chemotactic behavior of cells exposed for 10 min to a linear fMLP gradient with $\Delta C = 1$ nM. Fig. 1*A* shows the results, interpreted in terms of the chemotactic index (CI), which is the ratio of the distance traveled in the correct up-gradient direction to the total length of the cell migration path during the same period. The CI value for each individual cell is shown in relation to C_s over the range of 5–45 nM. To our knowledge, no previous study of chemotaxis has assessed behavior of each individual cell in relation to its starting position in the gradient.

CI is at its highest mean value (0.4) at the lowest testable C_s; no ascending portion of the curve was detected (Fig. 1*A*). From that point CI steadily decreases as C_s increases, becoming virtually indistinguishable from zero for cells that start at C_s >30–40 nM. Because ΔC remains constant in the linear profile, whereas C increases, we suspected that the progressive decrease in CI reflected a decrease in the cells' ability to sense and interpret constant ΔC at higher C.

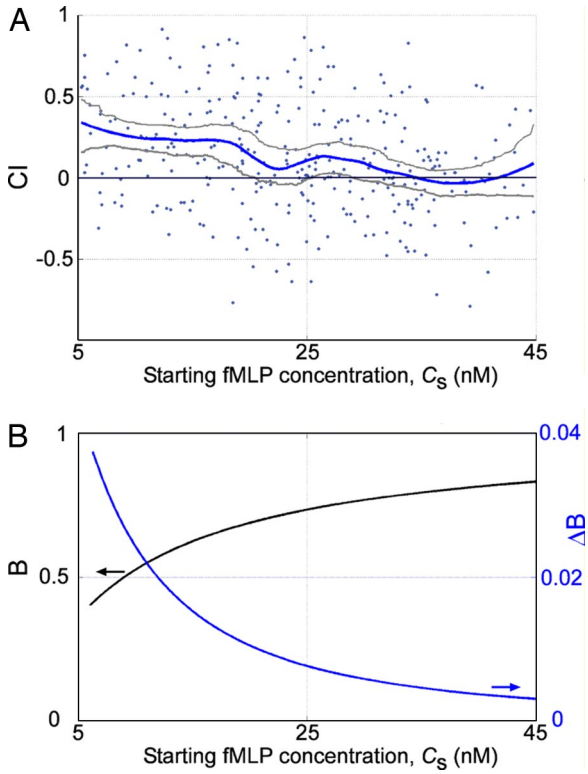

Fig. 1. Chemotaxis in a linear concentration profile of fMLP. (*A*) Chemotactic index (CI) as a function of the starting fMLP concentration, C_s. Blue dots indicate the CI values of individual cells, and the blue curve depicts the mean CI, computed by using a smoothing algorithm (see *SI Text*). Gray lines indicate the limits of 95% confidence intervals. (*B*) The mean fraction of occupied receptors, (B, black line), and difference in the fraction of occupied receptors across a cell with a diameter of 10 μm (ΔB, blue line) as functions of C_s for K_d = 10 nM, according to the proposed theoretical model. C_s is assumed to vary linearly from 5 to 45 nM fMLP over 400 μm.

The most likely reason for such a loss of sensitivity is that dHL60 cells use saturable receptors on their surfaces to detect and interpret both the mean C and differences in C across the cell's diameter. Binding studies have reported K_d for fMLP receptors in the range of 1–15 nM (18–21). With such K_d values, receptors become increasingly saturated as C_s increases from 5 to 45 nM, thereby reducing their sensitivity to variations of C. The resulting high degree of receptor saturation as C_s reaches 30–40 nM would explain the reduction of chemotactic prowess to an undetectable level.

We thus propose, and later test, a straightforward model in which the fraction of receptors bound to fMLP at any point on the cell's surface obeys the equation, $B = C/C + K_d$. In this model, the difference in the receptor occupancy between the front and back of a cell ($B_f - B_r$) is $\Delta B \approx (K_d/(C_s + K_d)2)\Delta C$ [see supporting information (SI) *Text* (*Basic Equations* and *Models*) and SI Table 2]. If we further assume that CI increases steadily with ΔB, then this equation predicts that ΔB, and therefore CI, will decrease as C_s increases at constant ΔC, exactly the behavior observed in the linear profile (Fig. 1*A*). Conceptually, this model is almost identical to a model discussed by Zigmond in 1981 (22). To illustrate predictions of this model, we can assume K_d at 10 nM. Then, at $\Delta C = 1$ nM, over the range of C_s shown in Fig. 1*A* (5–45 nM), ΔB would decrease 13.3-fold, from ≈0.04 to ≈0.003

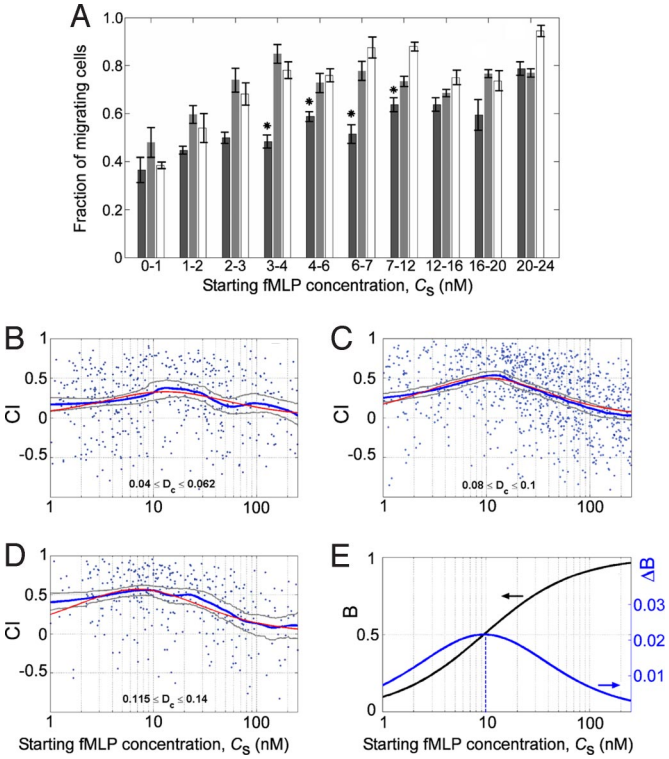

Fig. 2. Chemotaxis and migration in exponential gradients. (*A*) Effect of D_c on the likelihood of cells to migrate, as a function of starting fMLP concentration, C_s. Black, gray, and white bars indicate the fraction of cells that migrated at D_c values of 0.05, 0.09, and 0.13, respectively. Numbers on the abscissa indicate the range of C_s values of cells represented by each set of three bars. Cells in each D_c regime were separated into bins of different C_s, and the fraction of migrating cells was calculated for each bin. Each bin included data from multiple experiments (5–22 experiments, all performed on different days), with at least seven cells from every individual experiment. Error bars are ±1 SEM. For bins indicated by asterisks, which are in the region between 3 and 12 nM, the fractions of migrating cells in the low D_c regime were significantly less ($P < 0.05$) than in either of the two higher D_c regimes. (*B–D*) CI as a function of C_s for cells that move >20 μm. Curves are plotted for the three D_c regimes: respectively, 0.05 (n = 476 cells) (*B*); 0.09 (n = 1,023 cells) (*C*); and 0.13 (n = 372 cells) (*D*). Each blue line depicts the average trend in the data, computed from the CI of individual cells (blue dots) by using a smoothing algorithm. Gray lines show the 95% confidence intervals. The red line is the postulated theoretical relationship, CI = $k\Delta B$. (*E*) Theoretical fraction of occupied receptors, B (black) and difference in the receptor occupancy across one cell diameter, ΔB (blue) in an exponential gradient, as functions of C_s at K_d = 10 nM and D_c = 0.09.

(green line, Fig. 1*B*). If the model is correct, a decrease of ΔB and CI with C_s will always be seen for cells exposed to a given linear concentration profile.

Exponential Gradients. The ΔB-based model makes quite different predictions for exponential profiles, in which D_c is constant, whereas C_s and ΔC increase exponentially as a function of position in the gradient. We performed chemotaxis experiments in exponential profiles with different values of D_c (Fig. 2), which were created by using three different microfluidic devices (described in *Materials and Methods* and *SI Text*) with specially designed gradient-making networks (23).

The difference in receptor occupancy across a cell at its starting position in the gradient is given by $\Delta B \approx K_d/(C_s + K_d)^2 \cdot \Delta C = K_d C_s/(C_s + K_d)^2 \cdot \Delta C/C_s = K_d C_s/(C_s + K_d)^2 \cdot D_c$. Because exponential gradients maintain D_c constant, ΔB can be approximated by $\Delta B \approx K_d C_s/(C_s + K_d)^2 \cdot constant$. This function increases between $C_s = 0$ and K_d, reaches its maximum at K_d, and steadily decreases at higher C_s values (Fig. 2*E*). Dependence of CI on C_s should have the same general form, providing that, as the model suggests, CI is an increasing function of ΔB.

In 73 separate experiments with exponential profiles at different D_c values (see *Materials and Methods*), we tracked migration trajectories of cells exposed for 10 min to a range of attractant concentrations (1–250 nM fMLP). Because D_c varied somewhat between experiments, even with the same device and the same concentrations of fMLP fed to inlets in the device, we grouped experiments at different D_c values into three clusters: low D_c (mean = 0.05, range 0.04–0.062, 476 tracked cells; Fig. 2*B*); medium D_c (mean = 0.09, range 0.08–0.10, 1,023 tracked cells; Fig. 2*C*); and high D_c (mean = 0.13, range 0.115–0.14, 372 tracked cells; Fig. 2*D*).

To quantify chemotactic prowess, we first divided cells into two groups, "migrating" and "nonmigrating," depending on whether they moved within 10 min by more or <20 μm (two cell diameters) from their point of origin. As expected, the fraction of migrating cells strongly depended on C_s (Fig. 2*A*). At low C_s (<2 nM), only 40–50% of the cells migrated >20 μm, regardless of D_c (or ΔC). At C_s >20 nM, higher proportions of cells (75–90%) of cells migrated farther than 20 μm, again regardless of D_c or ΔC. Surprisingly, however, migration of cells at intermediate C_s values (3–12 nM) was strongly augmented by higher values of D_c and ΔC. In particular, in the low D_c regime only 50–60% of cells starting at C_s between 3 and 7 nM migrated further than 20 μm, but 80–90% of cells in the two higher D_c regimes did so, at the same C_s. Tracking individual cells revealed another difference (SI Fig. 4): many nonmigrating cells at the low D_c failed to move at all; in contrast, most of the nonmigrating cells at the medium and high D_c were detectably displaced from their starting positions, although usually by less than a single cell diameter.

Cells make the decision to migrate before they have a chance to explore their environment on scales larger than their diameter and to detect the presence of a gradient by sensing temporal changes in C as they move. Consequently, the decision to move can depend only on the properties of the field of concentration on the scale of the cell, C_s and D_c (or ΔC). Enhancement of cell motility by higher D_c at a given C_s thus indicates that cells directly sense variations of fMLP concentrations over their diameter. In other words, their gradient sensing can be purely spatial. The fact that the dependence of motility on D_c is strongest at C_s near K_d is consistent with the mathematical model introduced above, $\Delta B \approx K_d C_s/(C_s + K_d)^2 D_c$. Indeed, the effect of variation of D_c on ΔB is strongest when $C_s = K_d$, because at this concentration the factor by which D_c is multiplied, $K_d C_s/(C_s + K_d)^2$, is largest.

Once cells do initiate migration, how do they direct their course relative to the direction of the gradient? Fig. 2 *B–D* shows mean CI as a function of C_s at low, medium, and high D_c values, over a C_s range of 1–250 nM. In each D_c regime, CI rises to a peak and falls progressively thereafter. These peaks are seen within a rather narrow range of C_s: 13, 13, and 8.6 nM for low, medium, and high D_c regimes, respectively. The mean CI value at the peak increases progressively with D_c, from 0.38 at D_c = 0.05 (Fig. 2*B*) to 0.56 at D_c = 0.13 (Fig. 2*D*). [Note: data in Fig. 2 *B–D* exclude all nonmigrating cells, on the grounds that short trajectories of these cells make it impossible to assess CI accurately (see *SI Text*).]

At each value of D_c, the pattern of dependence of CI on C_s (blue lines in Fig. 2 *B–D*) agrees with the ΔB-based model in that CI increases at low C_s, decreases at high C_s and is maximal at values of C_s that are within the reported range of K_d (1–15 nM). Thus, the experimental results support the central element of the model, i.e., that chemotactic prowess, CI, depends on ΔB at the cell's starting concentration (C_s).

Our model need not make specific assumptions about exactly how CI depends on ΔB, apart from it being an increasing function. When spatial cues (ΔC and D_c) are weak and both ΔB

Table 1. Least-squares fits of CI to C_s

D_c	k (95% confidence bounds)	K_d (95% confidence bounds)	R^2	Adjusted R^2	RMSE
0.04–0.065	26.8 (26.4–27.3)	13.4 (12.9–13.8)	0.7201	0.7195	0.04162
0.08–0.10	23.2 (22.9–23.5)	8.5 (8.2–8.7)	0.904	0.9039	0.04918
0.115–0.14	19.3 (19,19.63)	7.5 (7.2,7.9)	0.7925	0.7919	0.07024

The experimental data shown in Fig. 2 *B–D* were fitted to the function $CI = k{\cdot}\Delta B = k{\cdot}[K_dC_s/(C_s + \Delta C + K_d)(C_s + K_d){\cdot}D_c] = k{\cdot}[C_s(1 + D_c)/[C_s(1 + D_c) + K_d] - C_s/(C_s + K_d)]$. Fitting parameters, K_d and k, were chosen by the algorithm independently for the three D_c ranges. The data include only cells that move >20 μm from their origin.

and CI are small, it is natural to suggest that CI may increase linearly with ΔB. Such a linear regime could prove difficult to establish experimentally, however, because small directional biases in cell migration (low CI) are difficult to assess accurately. In contrast, when chemotactic prowess is high, dependence of CI on ΔB should be a nonlinear function, which becomes increasingly saturated as CI reaches values close to unity. Indeed, for CI = 0.38 at $C_s = K_d$ and $D_c = 0.05$, a linear dependence of CI on ΔB would produce a CI value of 1.53 at $D_c = 0.2$; that cannot be correct, because CI by definition is always <1.

Nonetheless, approximating CI as a linear function of ΔB, $CI = k\Delta B \approx k{\cdot}K_dC_s/(C_s + K_d)^2{\cdot}D_c$, is useful for testing the general agreement of the model with the experimental results. We fitted the experimental data obtained in each D_c regime with this function (red curves in Fig. 2 *B–D*), considering k and K_d as independent fitting parameters. The best fits were obtained for K_d at 13.4, 8.4, and 7.5 nM fMLP for $D_c = 0.05$, 0.09, and 0.13, respectively (Table 1). All three values of K_d fall within the reported range of K_d and are close to the values of C_s at which the corresponding experimental dependencies have their maxima.

The convention of a linear relation between CI and ΔB also makes it possible to estimate how well the experimental data correlate with the ΔB model. For instance, the values of the coefficient of determination, R^2, show that the model accounts for 72, 90, or 79% of the trends relating CI to C_s at low, medium, and high D_c regimes, respectively (Table 1). Moreover, fits based on the approximation $CI = k\Delta B$ result in small values of the root mean square error, RMSE (Table 1), indicating that the fits are quite close to the experimental curves. The limitations of the linear approximation are manifested in the variation of the values of k providing the best fit: k decreases from 26.8 to 19.3 as D_c increases from 0.05 to 0.13. (The decrease of k with D_c is consistent with the expected nonlinear dependence of CI on ΔB and with the saturation of CI at large ΔB.)

We further note that the experimental data suggest that chemotactic prowess can also depend on factors that are not included in the current model. The curve of ΔB vs. C_s is symmetric with respect to K_d when plotted in semilogarithmic coordinates (Fig. 2*E*), so the shapes of CI vs. C_s curves obeying the ΔB model (both linear and nonlinear) should be symmetric with respect to K_d as well. The experimental data in all three D_c regimes show an apparent asymmetry, however, with CI declining faster at $C_s > K_d$ than at $C_s < K_d$. A likely reason for this asymmetry is that the mean receptor occupancy, $B = C_s/C_s + K_d$, is increasing with C_s, and the detection of ΔB becomes less efficient and reliable as the mean value of B increases. [This subject is further discussed in *SI Text* (*Theoretical Models of the Dependence of Chemotaxis on the Gradient and Ambient Concentration of fMLP*) and SI Table 3.] The asymmetry of the experimental curves probably accounts for the fact that the putative K_d values obtained from the fitting are all smaller than the values of C_s at the peaks of experimental curves.

The CI is the ratio of two independent parameters: the mean displacement of cells in the direction of the gradient and the contour length of the migratory path. The displacement parameter, which is an alternative measure of chemotactic prowess, behaves like CI in that it is higher at $D_c = 0.09$ and 0.13 than at $D_c = 0.05$ and in that the displacement is maximal at C_s near the putative K_d (SI Fig. 5). Peaks of the mean displacement curves, however, are broader that those of CI and are somewhat shifted toward higher C_s values. The second parameter, length of the cell's migratory path, reflects the overall motility of cells. The patterns seen with CI (Fig. 2) or with displacement in the correct direction (SI Fig. 6) do not resemble the pattern of variations in this second parameter (SI Fig. 7). Each parameter is of interest in its own right, and identifying their individual roles is a task for future experiments.

Discussion

The first important observation in our experiments is simple: chemotactic prowess depends on both the variation in attractant concentration in space (represented by ΔC) and the ambient concentration of attractant (represented by C_s). To observe the variation of chemotaxis with C_s, it was crucial to perform quantitative experiments using a fluorescent marker mixed with fMLP: this allowed us to measure the actual shape of the gradient and to determine C_s for each individual cell trajectory we analyzed (see *SI Text*). Chemotactic prowess (measured by CI) should depend on C_s, of course, because a cell's attractant receptors are saturable and limited in number. As the ambient concentration of fMLP, C, increases, an increasing number of receptors becomes occupied, thereby limiting the cell's ability to detect further increases in C.

Three decades ago, Zigmond (5) showed that neutrophils exposed to a slowly forming gradient of attractant orient themselves, over a time period of 30 min, in the up-gradient direction, and do so most efficiently at attractant concentrations near the K_d. The results of Zigmond's experiments fitted a model she devised (22), which is very similar to the ΔB model we used. The actual data, however, was limited by the performance of the chemotaxis chamber used to generate the gradient. The ambient attractant concentration was specified with a low precision (up to a 3× range at best), and the shape of the gradients was poorly defined and varied in the course of the assays. More recently, chemotaxis of various eukaryotic cells was studied in well defined concentration profiles in microfluidic devices (8–10, 12, 14, 24, 25). Those studies, however, have usually reported chemotactic responses of large cell populations exposed to relatively broad ranges of ambient attractant concentrations, without reference to the local concentration for individual cells.

Our second key conclusion is that neutrophil-like dHL60 cells are capable of sensing differences in attractant concentrations across their diameters in relatively shallow gradients and of translating this purely spatial cue into a decision of whether or not to migrate. At C_s close to K_d, higher ΔC values in concentration profiles with higher D_c made cells much more likely to migrate (Fig. 2*E*). At a given C_s, a cell's decision to migrate significantly depended on a small difference in the spatial cue to which it was exposed: the change from 5% to 9% (from $D_c = 0.05$ to $D_c = 0.09$) in the increment of attractant concentration between the back and the front of the cell.

The ability of dHL60 cells to interpret gradients purely spatially, without comparing attractant concentration at different times, is in accord with the demonstrated capacity of immobilized dHL60 cells to accumulate PIP3 at the up-gradient edge (2). It is nonetheless important to show that cells can not only sense spatial cues in a gradient, but can also translate those cues into an essential response, chemotactic migration. It is, moreover, not certain that PIP3 accumulation is the sole, or even the predominant, determinant of polarity and spatial orientation: pharmacologic inhibitors of PIP3 accumulation in dHL60 cells (26) or transgenic knockouts (27, 28) of a PIP3-degrading enzyme, PTEN, exerted a modest effect on chemotactic prowess. Knockout of a second PIP3-degrading enzyme, SHIP1, did impair chemotaxis (27), indicating that too much PIP3 can interfere with direction-finding but not that PIP3 normally plays a major role in guiding cells up gradients.

We further note that the dependence of motility on C_s is similar to the dependence of polarization on concentrations of fMLP, when the attractant is applied uniformly. For instance, 100 nM uniform fMLP induces 80–90% of dHL60 cells to polarize within 3 min, whereas 3 nM fMLP induces only 20% to do so; an intermediate fMLP concentration (10 nM) induces an intermediate proportion (≈50%) of cells to polarize (results not shown). This correlation between polarization and motility responses suggests that in addition to improving motility, application of larger gradients probably also increases the fraction of cells that polarize.

Our third major conclusion is that chemotaxing cells behave as if they interpret gradients primarily with the use of saturable receptors to assess differences in the attractant concentration across their own diameters. More specifically, the major features of the chemotactic response of cells are well described by a simple model, in which chemotactic prowess is an increasing function of the absolute difference in receptor occupancy, ΔB, at the front of the cell vs. the back of the cell. As the model predicts, chemotactic prowess (assessed by CI) in a linear concentration profile steadily decreases with C_s (Fig. 1*B*). Results with exponential concentration profiles (Fig. 2 *B–D*) provide even stronger evidence supporting the model. In all three tested ranges of D_c, the dependencies of CI on C_s agree with the model prediction: CI increases at low C_s, decreases at high C_s, and reaches a maximum near at C_s values very close to K_d.

The experimental results show that chemotactic prowess depends on C_s in gradients that maintain either ΔC or D_c constant, that is, in linear or exponential gradient profiles. Hence, although both ΔC and D_c can be considered essential spatial cues, neither suffices on its own to specify chemotactic prowess. Instead, the experimental results agree with the model's suggestion that chemotactic prowess depends on ΔB, defined by the expression $\Delta B \approx K_d/(C_s + K_d)^2 \cdot \Delta C = K_d C_s/(C_s + K_d)^2 \cdot D_c$. It is worth emphasizing that we know very little about the precise dependence of CI on ΔB, except that it is expected to be an increasing function, cannot be linear, and must reach saturation when CI is equal to unity. Moreover, we do not know whether or how the relation between CI and ΔB may depend on duration of exposure to the gradient, and we are at present too ignorant of the biochemical events involved to probe that relation with appropriate molecular perturbations. Clearly, further experiments will be required to explore the relation of CI to ΔB.

Several caveats are in order. First, we note that the experimental results have appreciable margins of error and do not exclude other models based on spatial gradient sensing by saturable receptors. In *SI Text* we discuss an alternative spatial sensing model, similar to a model previously proposed by Tranquillo *et al.* (29), which incorporates contributions of mean receptor occupancy and molecular noise. In addition, conformation of CI curves to a model that relates ΔB to ΔC, C_s, and K_d does not by any means imply that the initial ΔB of a cell

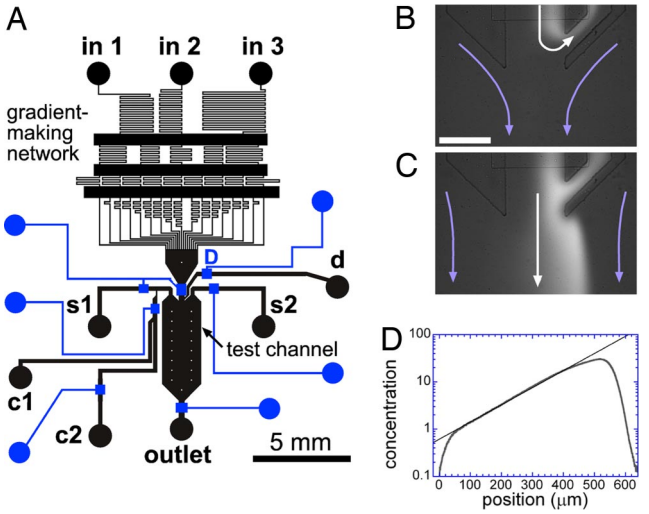

Fig. 3. Design and operation of the microfluidic device producing an exponential profile with $C_{high}/C_{low} = 81$. (*A*) Layout of microchannels in the flow layer (black) and control layer (blue). The ratio of concentrations of attractant (and fluorescein) fed into inlets in 1, in 2 and in 3 is 1:9:81. (*B* and *C*) Micrographs of the central part of the beginning of the test channel (under mixed bright-field/fluorescence illumination) illustrating operation of the device with a 50-ppm fluorescein solution fed to in 3. White arrows show the direction of the stream coming from the gradient-making network. Blue arrows indicate the sheath flow from s1 and s2. In *B*, valve D is open, and the gradient stream is diverted to port d. In *C*, D is closed, and the gradient stream is injected into the test channel. (*D*) Profile of concentration in the central part of the test channel (≈300 μm from the beginning) at a mean flow velocity of 150 μm/s in semilogarithmic coordinates. The concentration is normalized to the solution injected into 1. The profile is close to an exponent (the straight line) in a region ≈400 μm in width.

exposed to an fMLP gradient completely defines its subsequent chemotactic response. Certainly, cells must continue to assess ΔC and C as they migrate, and respond accordingly. In particular, the cell may augment its spatial gradient interpretation with a temporal strategy, in which the local values of C are compared at different times during the migration of the cell. Combining temporal and spatial modes of gradient interpretation would be in keeping with nature's frequent tendency to solve important problems by employing redundant, overlapping mechanisms. Our experiments do not test this possibility.

Finally, we note that none of the major findings of this work could have been made without the use of microfluidic devices, which expose cells to well characterized, stable gradients of attractant (*Materials and Methods* and *SI Text*). The stable gradients were applied in very short time intervals (1–3 sec), setting a well defined time point for initial exposure for all cells in each experiment. Moreover, the interval between the application of fMLP to the front and back of individual cells was <0.05 sec (see *SI Text*), thus reducing to a minimum the initial temporal component of the stimulus applied to the cells. Another key element of these experiments was the use of exponential concentration profiles, produced by specially designed microfluidic networks. Our experiments, the first to apply exponential profiles to analysis of chemotaxis, show that such profiles make it much easier to distinguish separate roles of the gradient and the ambient concentration. In addition, the exponential profiles made it possible to validate an important prediction of the proposed model, that CI at constant D_c is maximal at C_s near K_d.

Exponential concentration profiles have a number of practical advantages for studying chemotaxis. As we have shown, chemotaxis in linear profiles is most efficient at the low concentration

edge, where the actual profile differs from its designed shape because of diffusive smearing and other edge effects (23). These edge effects set a lower limit on the range of reliably accessible C_s at any given ΔC. In contrast, in exponential profiles, chemotaxis is most efficient near $C_s = K_d$ that can always be placed in the middle of the gradient-carrying stream by choosing appropriate concentrations at the edges. Therefore the range of accessible C_s is unlimited at any D_c. Finally, exponential profiles can furnish a rather wide region of concentrations, near $C_s = K_d$, in which chemotactic prowess is mainly defined by D_c and is almost independent of C.

Materials and Methods

Methods used in this study, including propagation and differentiation of HL60 cells, their introduction into the microfluidic devices, tracking of cells, quantitation of gradients and chemotaxis, and statistical analysis (including smoothing and linear regression), are described in *SI Text*.

Microfluidic devices used in this study (Fig. 3 and SI Figs. 8–10) comprise two main elements: the test channel, where the chemotaxis of dHL60 cells is analyzed, and the gradient-making network. The gradient-making network is fed by two or three source solutions with different concentrations of fMLP and generates a steady stream with a stable fMLP gradient of desired shape across the stream (7, 23). The gradient stream is either diverted into a designated outlet (d in Fig. 3*A*) or directed into the test channel (Fig. 3 *B* and *C*). The injection of the gradient stream into the test channel sets the time point of exposure of the dHL60 cells to the fMLP gradient (SI Fig. 9) and begins a chemotaxis assay. In the test channel, the gradient stream is squeezed in a sheath flow between two streams of plain buffer (Fig. 3*C*) coming from two auxiliary inlets (s1 and s2 in Fig. 3*A*). The magnitude of the gradient is inversely proportional to the width of the gradient stream, and the width is adjusted to vary the gradient (SI Fig. 9). The microfluidic device has seven integrated membrane valves that, when pressurized, locally seal the microchannels beneath them (11). The valves enable fast switching of the flow, easy loading of dHL60 cells into the test channel (from a dedicated inlet, s1 in Fig. 3*A*), incubating cells in the test channel without flow, and preventing premature exposure of the cells to fMLP. These features provided by the valves were critical for conducting the extensive series of repeatable experiments and collecting data on the large number of cells chemotaxing in different gradients.

This study used four different devices (Fig. 3*A* and SI Fig. 8) with gradient-making networks that generated a linear concentration profile (7) and three types of exponential profiles (23), in which the ratios between concentrations at the high and low concentration edges, C_{high}/C_{low}, were 16:1, 81:1, and 256:1. A higher value of C_{high}/C_{low} at a given profile width, w, results in larger fractional difference of concentration across a cell, $D_c = \ln(C_{high}/C_{low})\cdot L/w$, where $L = 10$ μm is the cell diameter. By varying the actual values (but not the ratio) of C_{high} and C_{low} in each of the three exponential devices, we could expose cells in different experiments to exponential profiles with a particular D_c but different (and overlapping) ranges of C. In this way, we assessed chemotaxis over a total range of attractant concentration substantially wider than achievable in any individual experiment. Diffusion across boundaries between the gradient and sheath streams caused gradient profiles to degrade at the edges, especially at the high concentration edge (Fig. 3 *C* and *D*). Nonetheless, the desired exponential shape was preserved within easily definable limits (Fig. 3 *C* and *D*). Here we report data only from those cells that remained within these limits along their entire migration trajectories.

We thank members of the H.R.B. laboratory for useful suggestions. A.G. is grateful to Steve Quake, Rick Firtel, and Ruedi Meili for help at initial stages of the project; to Herbert Levine for useful suggestions; and to Bill Loomis for introducing him to the subject of chemotaxis. This work was supported in part by National Institutes of Health Grant GM 27800 (to H.R.B.), a Nanotechnology Interdisciplinary Research Team grant from the National Science Foundation (to A.G.) and the Sandler Family Supporting Foundation (to H.E.-S.).

1. Berg HC (1988) *Cold Spring Harb Symp Quant Biol* 53 Pt 1:1–9.
2. Servant G, Weiner OD, Herzmark P, Balla T, Sedat JW, Bourne HR (2000) *Science* 287:1037–1040.
3. Janetopoulos C, Ma L, Devreotes PN, Iglesias PA (2004) *Proc Natl Acad Sci USA* 101:8951–8956.
4. Zigmond SH, Levitsky HI, Kreel BJ (1981) *J Cell Biol* 89:585–592.
5. Zigmond SH (1977) *J Cell Biol* 75:606–616.
6. Zigmond SH (1974) *Nature* 249:450–452.
7. Jeon NL, Dertinger SKW, Chiu DT, Choi IS, Stroock AD, Whitesides GM (2000) *Langmuir* 16:8311–8316.
8. Jeon NL, Baskaran H, Dertinger SK, Whitesides GM, Van de Water L, Toner M (2002) *Nat Biotechnol* 20:826–830.
9. Lin F, Nguyen CM, Wang SJ, Saadi W, Gross SP, Jeon NL (2004) *Biochem Biophys Res Commun* 319:576–581.
10. Lin F, Nguyen CM, Wang SJ, Saadi W, Gross SP, Jeon NL (2005) *Ann Biomed Eng* 33:475–482.
11. Unger MA, Chou HP, Thorsen T, Scherer A, Quake SR (2000) *Science* 288:113–116.
12. Irimia D, Liu SY, Tharp WG, Samadani A, Toner M, Poznansky MC (2006) *Lab Chip* 6:191–198.
13. Wang SJ, Saadi W, Lin F, Minh-Canh Nguyen C, Li Jeon N (2004) *Exp Cell Res* 300:180–189.
14. Song L, Nadkarni SM, Bodeker HU, Beta C, Bae A, Franck C, Rappel WJ, Loomis WF, Bodenschatz E (2006) *Eur J Cell Biol* 85:981–989.
15. Paliwal S, Iglesias P, Campbell K, Hilioti Z, Groisman A, Levchenko A (2007) *Nature* 446:46–51.
16. Isbister CM, Mackenzie PJ, To KC, O'Connor TP (2003) *J Neurosci* 23:193–202.
17. Xu J, Wang F, Van Keymeulen A, Herzmark P, Straight A, Kelly K, Takuwa Y, Sugimoto N, Mitchison T, Bourne HR (2003) *Cell* 114:201–214.
18. Mehta J, Spilberg I (1983) *Inflammation* 7:301–309.
19. Atkinson YH, Marasco WA, Lopez AF, Vadas MA (1988) *J Clin Invest* 81:759–765.
20. Tennenberg SD, Zemlan FP, Solomkin JS (1988) *J Immunol* 141:3937–3944.
21. Quehenberger O, Prossnitz ER, Cavanagh SL, Cochrane CG, Ye RD (1993) *J Biol Chem* 268:18167–18175.
22. Zigmond SH (1981) *J Cell Biol* 88:644–647.
23. Campbell K, Groisman A (2007) *Lab Chip* 7:264–272.
24. Walker GM, Sai J, Richmond A, Stremler M, Chung CY, Wikswo JP (2005) *Lab Chip* 5:611–618.
25. Dertinger SKW, Chiu DT, Jeon NL, Whitesides GM (2001) *Anal Chem* 73:1240–1246.
26. Van Keymeulen A, Wong K, Knight ZA, Govaerts C, Hahn KM, Shokat KM, Bourne HR (2006) *J Cell Biol* 174:437–445.
27. Nishio M, Watanabe K, Sasaki J, Taya C, Takasuga S, Iizuka R, Balla T, Yamazaki M, Watanabe H, Itoh R, *et al.* (2007) *Nat Cell Biol* 9:36–44.
28. Subramanian KK, Jia Y, Zhu D, Simms BT, Jo H, Hattori H, You J, Mizgerd JP, Luo HR (2007) *Blood* 109:4028–4037.
29. Tranquillo RT, Lauffenburger DA, Zigmond SH (1988) *J Cell Biol* 106:303–309.